PHYSICAL REVIEW B **92**, 064411 (2015)

Intracluster interactions in butterfly $\{Fe_3LnO_2\}$ molecules with the non-Kramers ions Tb(III) and Ho(III)

L. Badía-Romano,[1,2,*] J. Rubín,[1,3] F. Bartolomé,[1,2] J. Bartolomé,[1,2] J. Luzón,[1,4] D. Prodius,[5] C. Turta,[5,†] V. Mereacre,[5] F. Wilhelm,[6] and A. Rogalev[6]

[1]*Instituto de Ciencia de Materiales de Aragón. CSIC-Universidad de Zaragoza, E-50009 Zaragoza, Spain*
[2]*Departamento de Física de la Materia Condensada, Universidad de Zaragoza, E-50009 Zaragoza, Spain*
[3]*Departamento de Ciencia de Materiales e Ingeniería Metalúrgica, Universidad de Zaragoza, E-50018 Zaragoza, Spain*
[4]*Centro Universitario de la Defensa, Academia General Militar, E-50015, Zaragoza, Spain*
[5]*Institute of Chemistry, Academy of Sciences of Moldova, MD-2028 Chisinau, Republic of Moldova*
[6]*European Synchrotron Radiation Facility (ESRF), F-38043 Grenoble, France*

(Received 22 May 2015; revised manuscript received 15 July 2015; published 6 August 2015)

The intracluster exchange interactions within the "butterfly" $[Fe_3Ln(\mu_3\text{-}O)_2(CCl_3COO)_8(H_2O)(THF)_3]$ molecules, where Ln(III) represents a lanthanide cation, have been determined by a combination of x-ray magnetic circular dichroism (XMCD) and vibrating sample magnetometry (VSM) along with an interaction model. We have studied the compounds with Ln = Tb and Ho, both non-Kramers lanthanides and with high uniaxial anisotropy, and Ln = Lu(III) and Y(III) as pseudolanthanides, which supply nonmagnetic Ln reference cases. At low temperature, the three Fe atoms can be considered as a self-unit with total spin $S_{Fe_3} = 5/2$. Using the element selectivity of the XMCD magnetometry, measured at the Ln $L_{2,3}$ edges, together with the VSM measurements, the local magnetization of the Ln ion and the Fe_3 subcluster, as a function of the field and low temperature ($T \approx 2.5$ K), has been determined separately. These results are described quantitatively in the framework of a theoretical model based on an effective spin Hamiltonian, which considers the competing effects of intracluster interactions and the external applied magnetic field. The Ln-Fe_3 exchange interaction within the $\{Fe_3LnO_2\}$ cluster has been determined to be antiferromagnetic, in both Tb and Ho compounds, with $\mathcal{J}_{FeTb}/k_B = -0.13(1)$ K and $\mathcal{J}_{FeHo}/k_B = -0.18(1)$ K, respectively. In both cases, a field-induced reorientation of the Fe_3 and Ln spins from antiparallel to parallel orientation takes place at a threshold field $\mu_0 H = 1.1$ and 2 T, for the $\{Fe_3TbO_2\}$ and $\{Fe_3HoO_2\}$ compounds, respectively. By comparison with other compounds of the series with uniaxial anisotropy, it is concluded that the polarizability of the Fe_3 subcluster magnetic moment decreases in the trend $\{Fe_3YO_2\} \rightarrow \{Fe_3TbO_2\} \rightarrow \{Fe_3HoO_2\} \rightarrow \{Fe_3DyO_2\}$, because of the increasing opposition of the exchange antiferromagnetic field caused by the Ln ion. In the Ln = Tb, Ho, and Dy, the magnetization of the whole molecule is dominated by the anisotropy of the Ln ion. The intracluster Fe_3-Ln exchange interactions are very weak compared to the Ln ligand field and Fe-Fe exchange interactions.

DOI: 10.1103/PhysRevB.92.064411 PACS number(s): 75.50.Xx, 75.10.Dg, 75.30.Et, 75.30.Gw

I. INTRODUCTION

Among the most fascinating aspects of magnetism in recent years, the discovery that the magnetic moment of individual molecules can give rise to magnetic hysteresis phenomena stands out. These systems have been called single molecule magnets (SMMs) [1–3]. Such physical systems have received much attention due to their intriguing physical properties and potential applications in high-density information storage [4] and quantum computing [5]. These molecular compounds exhibit slow relaxation of the magnetization below a certain blocking temperature, originating from the combination of a high spin ground state S and a large uniaxial anisotropy [6]. They create an anisotropy barrier between the spin-up and spin-down states high enough in comparison with the available thermal energy to hinder the thermally activated reorientations of the magnetic moment.

Lanthanide organic compounds containing 3*d* transition elements have been considered as especially promising candidates for developing high barrier SMMs. The main idea is to combine the magnetic moment and the relatively strong exchange interactions of 3*d* transition metals (M) with the anisotropy naturally provided by lanthanide ions (Ln) [6–9].

In a previous work [10], we investigated the magnetic interactions and field-induced spin reorientation in two compounds of the series $\{Fe_3LnO_2\}$ with Ln = Gd(III) and Dy(III), which correspond to the most extreme and opposite behavior as regards the magnetic anisotropy. In fact, Gd(III) is isotropic while Dy(III) shows the highest uniaxial anisotropy of the series, both lanthanides being ions with a half-integer-spin number, i.e., Kramers ions. In an experimental study combining x-ray magnetic circular dichroism (XMCD) and vibrating sample magnetometry (VSM), it was concluded that the Ln-Fe_3 subcluster interaction is antiferromagnetic with exchange energy of the order of 1 K. Besides, in an applied field, the magnetization of the whole molecule is dominated by the anisotropy of the Ln ion. The Fe_3 and Ln magnetic moments undergo an intramolecular spin reorientation as the applied field overcomes a threshold value.

In the present paper, we focus our attention on two particular cases of the $\{Fe_3LnO_2\}$ "butterfly" molecule series that contain a Ln ion which has an integer quantum number. This is the case of the non-Kramers ions Tb(III) and Ho(III). From *ab initio* calculations, we find that in these compounds

*lbadia@unizar.es
†Professor Turta passed away on the 23rd March 2015.

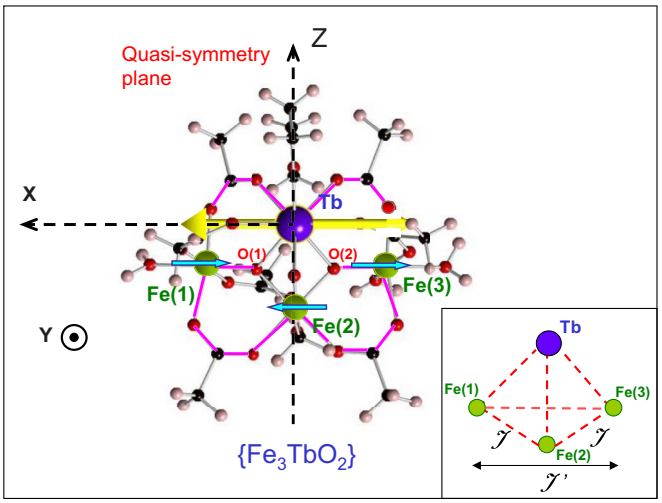

FIG. 1. (Color online) Structure of the $\{Fe_3TbO_2\}$ complex. Easy axis of magnetization of the Tb ion (yellow arrow), obtained from the *ab initio* calculations of the ground state. Blue arrows indicate the magnetic moment direction of the three Fe atoms, taking into account that an exchange interaction is acting between the Tb and Fe_3 spins. (Inset) Magnetic core of the $\{Fe_3TbO_2\}$ compound and definition of exchange parameters between the three Fe ions. The Y axis points outwards from the figure. The YZ plane forms the quasisymmetry plane.

the two lowest energy states are singlets separated by an energy Δ. Moreover, from those calculations we show that the Ln = Ho substitution is predicted to have uniaxial anisotropy with its easy anisotropy axis (EAM) direction close to the quasisymmetry plane of the molecule, as in the Dy case. In contrast, Tb has its EAM direction oriented perpendicular to the quasisymmetry plane of the molecule, which introduces uniaxial anisotropy in the x direction (see Fig. 1). A formalism to analyze the magnetic properties of these compounds using an effective spin Hamiltonian will be described. Those predictions are verified *a posteriori* by the sound fits obtained for the experimental data with the proposed model.

The Tb(III) and Ho(III) ions in transition metal clusters have been studied earlier in the context of the search for molecules that show SMM behavior [11–13]. Those studies have in common that they were performed using bulk techniques, such as magnetization and ac susceptibility measurements. A major problem intrinsic to this type of compounds is that their magnetic properties are complicated by the large spin-orbit coupling effects of the Ln(III) ions, hampering the quantitative elucidation of the magnitude of the exchange parameters within these molecules and their resulting ground-state description. Therefore new techniques are needed to provide information about the quantum state of magnetic moments and the mechanisms of relative spin orientation within a molecule. An example of these sensitive probes is the XMCD technique, which provides element specific magnetization curves [14,15].

In this work, the Ln-Fe_3 intracluster interaction has been studied by applying a competing external field and low temperatures to produce the polarization of the Fe and Ln magnetic moments. A detailed magnetic study involving XMCD at the Ln $L_{2,3}$ edges and VSM magnetometry has been done to characterize the exchange coupling and magnetic anisotropies of the present "butterfly" molecules. In particular, the evolution with the magnetic field of the local magnetization from the $4f$ states has been explored, both experimentally, by means of XMCD measurements as a function of the applied field at the Ln $L_{2,3}$ edges, and theoretically, by simulation of the Ln and Fe_3 subcluster magnetization dependence on applied field and temperature.

The $4f$ unpaired electrons dominate the magnetic behavior of the Ln ions. Since at the Ln $L_{2,3}$ edges the dominant XMCD signal corresponds to the $2p \rightarrow 5d$ transitions, only the magnetism originating from the $5d$ states is probed. However, due to the positive intra-atomic exchange coupling, the spin of the $5d$ electrons aligns parallel to the $4f$ ones [16], and therefore, the evolution with the field of the local magnetization from the $4f$ states can be determined since it is directly proportional to the amplitude of the XMCD signal at the $L_{2,3}$ edges.

The paper is organized as follows: the sample preparation, structural, and experimental details are given in Sec. II. The *ab initio* simulations performed on the present molecules are detailed in Sec. III. In Sec. IV, we describe the spin Hamiltonian model and approximations later used in the interpretation of the data. In Sec. V, the experimental results from XAS and XMCD at an applied field as well as the macroscopic magnetization are shown. The experimental results are compared to simulations performed with the theoretical model, and the exchange interaction parameters obtained are compared to those of Ln = Y and Dy in Sec. VI. Finally, the conclusions are presented in Sec. VII.

II. EXPERIMENTAL SECTION

A. Synthesis and structure

The chemical formula of the studied samples is $[Fe_3Ln(\mu_3\text{-}O)_2(CCl_3COO)_8(H_2O)(THF)_3]$, where Ln represents the lanthanide ions Tb(III) and Ho(III). The synthesis of the compounds is briefly reviewed on Refs. [17,18]. The molecular structure of the $\{Fe_3TbO_2\}$ complex is shown in Fig. 1 as an example. The tetranuclear entity has a "butterfly" type structure, with two $Fe_2Ln(\mu_3\text{-}O)$ triangular wings sharing a Ln-Fe body and a dihedral angle between the wings of 146.5°. Though the molecule symmetry is as low as the group C_1, a quasisymmetry plane can be defined by the "butterfly" body and a perpendicular axis, i.e., the yz plane, and x axis in Fig. 1. The metals are bridged by two μ_3-oxo centers and eight carboxylate ligands. The bond distances and angles for the Ho compound are given in Ref. [19]. Each Fe atom has a distorted octahedral coordination environment formed by six oxygen donor atoms. However, the precise donor set is different for each iron, being the environment of Fe(1) and Fe(3) closely similar, whereas that of Fe(2) is significantly different. Fe(1) and Fe(3) are located at the wing tips and are denoted as Fe_w, while Fe(2), in the body, is designated Fe_b. The magnetic core of the molecule can be considered as a triangular pyramid where the basis is an obtuse isosceles triangle with three Fe(III) located at the vertices, and Ln located at the pyramid apex [Fig. 1(inset)].

CCDC 721164 contains the supplementary crystallographic data for the $\{Fe_3HoO_2\}$ complex.[1]

B. Magnetic and XMCD measurements

The samples of the $\{Fe_3LnO_2\}$ series of compounds are powders, therefore, both bulk magnetometries and XMCD do measure the orientationally averaged projection of the magnetization along the applied magnetic field. The total magnetization of the molecule was measured on randomly oriented powder mixed with daphne oil on a PPMS measurement platform with a vibrating sample magnetometer (VSM) option, at a temperature of 2.7 and 2.2 K and a field up to 14 T, for the Tb and Ho compounds, respectively. The excitation frequencies were varied within the range from 10 to 1500 Hz.

The magnetization obtained with the XMCD magnetometry is that of the x-ray absorbing sublattice, which is selected by tuning the monochromator to a given energy edge. The XMCD experiments were performed at the ID12 beamline of the ESRF, dedicated to polarization dependent x-ray spectroscopy in the energy range from 2 to 20 keV [20], covering the energy of the $L_{2,3}$ edges of Tb (7.5–8.4 keV) and Ho (8–9 keV). In these experiments, it is the 2nd harmonic of the HU-52 Helios-II undulator that generates the circular polarized x-ray photons. Then, a double-Si(111) crystal monochromatizes the incoming radiation with a polarization rate over 95% in all cases. The XMCD signal corresponds to the direct difference between two x-ray absorption near-edge structure (XAS) spectra recorded in a magnetic field, one measured with right circularly polarized light, and one with left circularly polarized light. Total fluorescence yield in backscattering geometry was used as detection technique. To minimize the radiation damage possibly affecting our samples, the brilliance of the beam incoming onto the sample was reduced by a factor 600 compared to the x rays provided by the 1st harmonic of Apple-II (typical undulator at the incident energy used) using the 2nd harmonic of the Helios-II helical undulator together with a set of Al and Cu attenuators. The samples were prepared as powder pellets of about 8 mm diameter and mounted on a sample holder that could be screwed tightly on the cold finger in a liquid helium flow cryostat inserted into a superconducting magnet, which can produce magnetic fields up to 17 T.

III. *AB INITIO* SIMULATIONS

In order to obtain the electronic level structure, the wave functions and the orientation of the main-anisotropy axes of the Ln(III) ions in the "butterfly" $\{Fe_3LnO_2\}$ molecules, relativistic *ab initio* calculations were performed. Post-Hartree-Fock calculations were carried out using the CASSCF/CASPT2-RASSI-SO [21] method as implemented in the MOLCAS 7.4 package [22]. Such a relativistic quantum-chemistry method has proven to be suitable for the study of the magnetic anisotropy of trivalent lanthanide ions and, in particular, to predict with good accuracy the direction of the easy anisotropy axis for lanthanide ions with uniaxial magnetic anisotropy [23–25].

Computations were done on a $[Fe_3Ln(\mu_3\text{-}O)_2(CCl_3COO)_8(H_2O)(THF)_3]$ molecular unit, in which the -CCl_3 groups were replaced by -CH_3 groups and the -OC_4H_8 groups linked to the Fe(III) ions by water molecules in order to reduce the computation time. In addition, the Fe(III) ions were replaced by Sc(III) ions in order to reduce the active space: Sc(III) are diamagnetic ions with a covalent radius similar to the Fe(III) one and with a similar coordination chemistry. Finally, the disorder of the cyclic THF ligand bound to Ln(III) was disregarded and an average ring geometry was used.

All the atoms were represented by a basis set of atomic natural orbitals from the ANO-RCC library, as implemented in the MOLCAS 7.4 quantum-chemistry package. The following contractions were used: $[8s7p4d3f2g1h]$ for Ln(III) atom, $[6s5p3d]$ for the Sc atoms, $[4s3p]$ for the O and C atoms linking the Ln(III) ion with the 3 Fe(III) ions and for the O and C atoms of the -OC_4H_8 group linked to the Ln(III) ion, $[3s2p]$ for the all the other C and O atoms and $[2s]$ for all H atoms.

State averaged CASSCF calculations of the ^{2S+1}L multiplet roots were computed and it was checked that other multiplets have no effect on the final results. The molecule symmetry is low, C_1, therefore it is not evident which might be the reference axis to describe the wavefunctions of the magnetic cluster. We developed a practical convention to tackle this problem in a systematic way.

As a first step we focused our attention on the Ln atom. Its site symmetry is C_1, so there is not a preferential symmetry axis. To determine the energy eigenvalues and eigenvectors of the $4f$ electrons in the molecule, *ab initio* calculations were performed. From the calculations the ground state $\hat{g}$ tensor of the Tb(III) and Ho(III) ion was obtained. In both cases the calculation yielded uniaxial symmetry, i.e., maximum value in one direction, $g_{\parallel}^{*}$, and $g_{\perp}^{*} = 0$ otherwise.

To describe these results with respect to the molecule, it is convenient to define a quasisymmetry plane defined by the bisector plane to the dihedral angle of the wings. The principal axis of the Ho $\hat{g}$ tensor is contained in this plane, and defines the reference z axis. The x axis is defined by the line perpendicular to the bisector plane that intersects at the Ln ion, while the y axis is determined by choosing the standard right-handed coordinate system $x \wedge y = z$ (see Fig. 1).

Since the Fe_3 group is magnetically isotropic, its electronic states can be defined with respect to this set of reference axes. Therefore the effective spin Hamiltonian of the magnetic cluster, the spin operators, and wave functions are described with respect to the same axes.

The lanthanide ion quantum states obtained by the *ab initio* calculations will be described as combinations of single ion angular momentum kets $|J_{\mathrm{Ln}}, M_J\rangle$. The simulations show that the Tb(III) ground state is constituted mainly by the $|J_{\mathrm{Tb}}, M_J\rangle = |6, \pm 6\rangle$ states and, to a lesser degree by $M_J = -4, -2, 0, 2, 4$ states. The contribution of states with odd M_J is negligible. The two lower energy states are singlets separated by a computed energy gap $\Delta/k_{\mathrm{B}} = 3.17$ K (see Fig. 5(a) and Table III of Ref. [26]). The next excited state lies at 106.5 K from the minimum energy state, which means

[1]These data can be obtained free of charge via http://www.ccdc.cam.ac.uk/conts/retrieving.html, or from the Cambridge Crystallographic Data Centre, 12 Union Road, Cambridge CB2 1EZ, UK; fax: (+44) 1223-336-033; or e-mail: deposit@ccdc.cam.ac.uk.

that at the experimental low temperatures the magnetic signal from the Tb(III) ion is only due to the two lowest energy states. Moreover, the calculations reveal a strong uniaxial anisotropy for the Tb ion, $\hat{g}^* = (17.5,0,0)$. Specifically, it predicts the direction of the easy axis of magnetization (EAM) as perpendicular to the quasisymmetry plane of the molecule (see Fig. 1 and Ref. [26]).

In the case of Ho(III) compound, the *ab initio* calculations predict a very anisotropic ground-state multiplet with an energy gap, $\Delta/k_B = 9.7$ K, between the two lowest energy states (see Ref. [26]), while the next excited state lies at 44 K from the minimum energy state. Moreover, these calculations reveal that the two lowest energy states are constituted by a similar proportion of states M_J (see Table IV of Ref. [26]). However, a large mixture of states M_J exists in the two lowest energy states. Indeed, it is constituted mainly by $|J_{Ho}, M_J\rangle = |8, \pm 8\rangle$, but other states also contribute: $|J_{Ho}, M_J\rangle = |8, \pm 6\rangle$, $|J_{Ho}, M_J\rangle = |8, \pm 3\rangle$, $|J_{Ho}, M_J\rangle = |8, \pm 1\rangle$. Moreover, the *ab initio* gyromagnetic factors along the three main single-ion anisotropy axes, $\hat{g}^* = (0,0,15.68)$, indicate a large uniaxial magnetic anisotropy, with its direction parallel to the quasisymmetry plane of the molecules.

For Tb and Ho ions, the *ab initio* calculations produced $\hat{g}$ tensors with a single nonzero component. This is consistent with the general result by Griffith [27] for a system with an even number of electrons and a quasidoublet of lowest states, that the doublet itself defines a unique axis (the principal axis) and $g_\perp = 0$ (Ref. [26]).

IV. THEORETICAL MODEL

The magnetic cluster $\{Fe_3LnO_2\}$ will be described as a binuclear system made of a subcluster Fe_3 and the Ln ion. Firstly, we analyze the magnetic contribution of the Fe_3 subcluster. The $M(H)$ and $\chi T(T)$ curves of the complexes $\{Fe_3LnO_2\}$ with Ln = Y and Lu, reported in Ref. [19], were interpreted in terms of a model which considers the three Fe atoms with an exchange interaction ($\mathcal{J}$ and $\mathcal{J}'$) acting between them (see inset of Fig. 1).

The spin Hamiltonian that describes the Fe_3 subcluster in the Heisenberg-Dirac-Van Vleck (HDVV) approximation is

$$\hat{H}_{Fe_3} = -2\mathcal{J}(\vec{S}_1 \cdot \vec{S}_2 + \vec{S}_2 \cdot \vec{S}_3) - 2\mathcal{J}'(\vec{S}_1 \cdot \vec{S}_3), \qquad (1)$$

where $\vec{S}_i$ with $i = 1,2,3$ are spin operators at each Fe atom ($S_i = 5/2$).

It was concluded that both exchange interactions $\mathcal{J}/k_B \simeq -50$ K between Fe_w-Fe_b are identical and antiferromagnetic (AF), while the interaction $\mathcal{J}'$ between Fe_w-Fe_w is negligibly small. It is important to remark that in this case, although being a three spin triangle with AF interaction, no frustration happens since the interaction between the Fe_w moments is negligible [19].

The Fe_3 subcluster magnetization, M_{Fe_3}, at $T = 1.8$ K has been fitted in terms of an isotropic effective $S_{Fe_3} = 5/2$, with $g = 1.9(1)$ (Ref. [10]), which we have included in Fig. 8. Though some anisotropy may still be present in the Fe_3 subcluster at the experimental temperature of this work, it will be considered negligible. The measured saturation value of $4.7\mu_B$ of the complexes $\{Fe_3LnO_2\}$ with Ln = Y and Lu, indicates that the ground state of the three Fe atoms in the cluster is that of three antiferromagnetically coupled Fe(III) $S = 5/2$ moments, yielding a total spin of the Fe_3 triangle of $S_{Fe_3} = 5/2$ [10,19]. Moreover, Mössbauer spectroscopy studies performed on these $\{Fe_3LnO_2\}$ complexes nicely confirmed that the total Fe_3 cluster spin is $S_{Fe_3} = 5/2$ [19]. Therefore the Fe_3 triangle can be considered as a robust magnetic self unit, with effective spin $S_{Fe_3} = 5/2$ and isotropic tensor $\hat{g}_{Fe_3} = 2$ at low temperature ($k_B T \ll \mathcal{J}$).

Secondly, we consider the magnetic state of the lanthanide ions Tb ($^7F_6$) and Ho ($^5I_8$). The ligand field (LF) interaction ($\hat{H}_{Ln}$) acting on the Ln(III) ion is taken into account in the cluster Hamiltonian if its strength is comparable to the corresponding exchange constant. In order to determine the splitting of electronic energy levels produced by the ligand field and their eigenfunctions, *ab initio* calculations were performed, as explained in Sec. III.

Working with the complete basis set $S_{Fe3} \bigotimes J_{Ln}$ of the coupled Fe_3 subcluster effective spin $2S_{Fe3} + 1$ and the lanthanide $2J_{Ln} + 1$ *ab initio* wave functions to compute eigenvalues for the total system is prohibitively long in computing time (total dimensions for Tb and Ho are 78 and 102, respectively). However, as explained below, at low temperature, we can work with an effective spin Hamiltonian to calculate the $M(H)$ of the Fe_3 and Ln subclusters separately.

At zero applied magnetic field, the *ab initio* calculations reveal that the non-Kramers ions Tb(III) and Ho(III) low-energy states consist of a ground singlet and an excited one at an energy Δ. They are linear combinations of $|J_{Ln}, \pm M\rangle = |J, \pm M\rangle$ angular momentum wave functions with respect to the quantization axis Z defined by the uniaxial anisotropy direction obtained from the nonzero $\hat{g}$ tensor component in the *ab initio* calculations for each particular rare earth. The next excited levels are two and one orders of magnitude higher in energy (E_2). Since the present experiments were carried out at low temperature ($k_B T \leqslant \Delta \ll E_2$), we will only consider the two lowest states. The ground-state wave function $|\xi_0\rangle = \sum_{M=-J}^{J} C_{J,M}^{(0)} |J,M\rangle$ and the first excited one $|\xi_1\rangle = \sum_{M=-J}^{J} C_{J,M}^{(1)} |J,M\rangle$ (the $C_{J,M}^{(i=0,1)}$ coefficients are given in Ref. [26] Tables III and V, for Tb and Ho ions, respectively) are eigenfunctions with the reference energy $E_0 = 0$, and $E_1 = \Delta$. Therefore, in the subspace spanned by these two states, the ligand-field Hamiltonian can be expressed as

$$\hat{H}_{Ln}^{s} = \Delta \begin{pmatrix} 0 & 0 \\ 0 & 1 \end{pmatrix}. \qquad (2)$$

For even-electron systems, like the Tb^{+3} and Ho^{+3} ions, Griffith [27] has shown that the behavior of their eigenfunctions under time-reversal symmetry along with the presence of a lowest energy doublet well separated from the excited states lead to uniaxial anisotropy, i.e., $g_z \neq 0$ and $g_x = g_y = 0$. Indeed, this result was obtained from the *ab initio* calculations at $H = 0$ applied field in the previous section.

For $H \neq 0$, we may still use the $\{|\xi_0\rangle, |\xi_1\rangle\}$ doublet. However, since both eigenfunctions contain both $|J, M = \pm J\rangle$ terms as their major contributions to the total wave function, it is useful to apply a basis change that maximizes the $\hat{J}_Z$ eigenvalues. This is achieved by a transformation R into a new

base $|\eta\rangle$, $|\zeta\rangle$,

$$|\eta\rangle = \frac{1}{\sqrt{2}}(|\xi_0\rangle + |\xi_1\rangle) \text{ and } |\zeta\rangle = \frac{1}{\sqrt{2}}(|\xi_0\rangle - |\xi_1\rangle) \quad (3)$$

for which

$$\hat{J}_Z|\zeta\rangle \simeq J|\zeta\rangle \text{ and } \hat{J}_Z|\eta\rangle \simeq -J|\eta\rangle \quad (4)$$

(see Ref. [26] Table IV and VI for Tb and Ho ions, respectively).

At high magnetic field, the Zeeman term of the Hamiltonian becomes diagonal by construction,

$$\hat{H}_Z^s = g_J \mu_B H \hat{J}_Z = g_J \mu_B H J \begin{pmatrix} 1 & 0 \\ 0 & -1 \end{pmatrix}, \quad (5)$$

while the ligand-field term becomes

$$\hat{H}_{\text{Ln}}^{'s} = R^{-1} \hat{H}_{\text{Ln}}^s R = \frac{\Delta}{2}\begin{pmatrix} 1 & 0 \\ 0 & 1 \end{pmatrix} + \frac{\Delta}{2}\begin{pmatrix} 0 & 1 \\ 1 & 0 \end{pmatrix}. \quad (6)$$

The two basis states [Eq. (3)] span a subspace in which the ligand field Hamiltonian can be expressed in terms of a fictitious $|1/2, \pm 1/2\rangle$ basis by the projection $|\zeta\rangle \rightarrow |1/2, +1/2\rangle$ and $|\eta\rangle \rightarrow |1/2, -1/2\rangle$ [28]. Then, the Zeeman and the ligand-field effective Hamiltonian can be expressed in terms of the Pauli matrices σ_i, $\hat{S}_z^* = \frac{1}{2}\sigma_z$, $\hat{S}_x^* = \frac{1}{2}\sigma_x$, and $\hat{S}_y^* = \frac{1}{2}\sigma_y$:

$$\hat{H}^* = ct + \hat{H}_Z^* + \hat{H}_{\text{Ln}}^* = ct + g_Z \mu_B H \hat{S}_Z^* + \Delta \hat{S}_X^*, \quad (7)$$

where $2g_J J = g_Z$, ct means constant term and X is perpendicular to the quantization axis Z, defined by the EAM obtained from the *ab initio* calculations. With respect to the axes x, y, and z of the molecule, for Tb, $Z = x$, $X = y$, while for Ho, $Z = z$, $X = x$. In what follows, all variables in the fictitious 1/2-spin representation will be tagged with an asterix (*).

The fictitious $S^* = 1/2$ introduced for the non-Kramers states is not identical to that of the Kramers doublets. In the non-Kramers case, the $\hat{S}_Z$ operator is time-odd with respect to time reversal, while the $\hat{S}_{X,Y}$ operators are necessarily time-even, while in a Kramers doublet all the spin components are time-odd. Since we are interested in calculating the magnetization under an applied field, which breaks time-reversal symmetry, we will apply the $S^* = 1/2$ approximation defined with respect to the Z axis direction obtained in the *ab initio* calculations.

Thus, in the $S^* = 1/2$ formalism and assuming a common quantization axis for the Ln and the Fe_3 subcluster, the anisotropic exchange interaction spin Hamiltonian can be expressed as

$$\hat{H}_{\text{Ln-Fe}_3}^* = -2 \sum_{\alpha=x,y,z} \mathcal{J}_{\text{FeLn},\alpha}^* S_{\text{Ln},\alpha}^* S_{\text{Fe}_3,\alpha}, \quad (8)$$

where $\mathcal{J}_{\text{FeLn},x}^*$, $\mathcal{J}_{\text{FeLn},y}^*$, and $\mathcal{J}_{\text{FeLn},z}^*$ are the diagonal terms of the anisotropic exchange interaction tensor. When $\mathcal{J}_{\text{FeLn},x}^* = \mathcal{J}_{\text{FeLn},y}^* = 0$, the Ising-type spin-spin interaction is obtained.

Under an applied magnetic field $\vec{H}$, both entities, the Fe_3 subcluster and the Ln ion, will be affected by the anisotropic Zeeman term,

$$\hat{H}_Z^* = (\hat{g}_{\text{Fe}_3} \mu_B \vec{S}_{\text{Fe}_3} + \hat{g}_{\text{Ln}} \mu_B \vec{S}_{\text{Ln}}^*) \cdot \vec{H}, \quad (9)$$

where $\hat{g}_{\text{Ln}}$ is the g tensor for the corresponding Ln ion.

The effective spin cluster Hamiltonian ($\hat{H}_{\text{cluster}}$) including the exchange interaction, the LF and the Zeeman term, is

$$\hat{H}_{\text{cluster}}^* = \hat{H}_{\text{Fe}_3} + \hat{H}_{\text{Ln}}^* + \hat{H}_{\text{Ln-Fe}_3}^* + \hat{H}_Z^*. \quad (10)$$

The basis wave functions of the Ln-Fe_3 cluster restricted to the use of the fictitious 1/2 spin were constructed by the product $\hat{J}^* = \hat{S}_{\text{Fe3}} \otimes \hat{S}_{\text{Ln}}^*$ of the Fe_3 subcluster and the fictitious spin $S_{\text{Ln}}^* = 1/2$ of the lanthanide ion,

$$|\phi_{i=1,12}\rangle = |S_{\text{Fe3}} = 5/2, m_{\text{Fe3}}\rangle |S_{\text{Ln}}^* = 1/2, m_{\text{Ln}}\rangle, \quad (11)$$

which can be described in terms of a total angular momentum J^* and its third component M_J^*: $|\phi_i\rangle \equiv |J^*, M_J^*\rangle$, $|S_{\text{Fe3}} + S_{\text{Ln}}^*| \geqslant J^* \geqslant |S_{\text{Fe3}} - S_{\text{Ln}}^*|$. Diagonalization of the Hamiltonian of Eq. (10) yields the energy eigenfunctions at $H = 0$ as lineal combinations of the $|J^*, M_J^*\rangle$ functions. A note of care should be mentioned here. Inherently to the method of construction of the $|S_{\text{Ln}}^* = 1/2, m_{\text{Ln}}\rangle$ functions, they are even with respect to time reversal. Then, since the $|S_{\text{Fe3}} = 5/2, m_{\text{Fe3}}\rangle$ are time-odd functions, the total function $|J^*, M_J^*\rangle$ is time-odd. In fact, at $H = 0$, the cluster states are Kramers doublets (see Ref. [26]) Table V and VIII, for Tb and Ho compounds, respectively.

The contributions to the total magnetization due to the Ln ion and the Fe_3 subcluster were simulated by finding the eigenfunctions of the total effective Hamiltonian $\hat{H}_{\text{cluster}}^*$ (see Sec. IV). The fictitious $S^* = 1/2$ approximation for the two lower energy states has the counterpart of losing the information from the excited states in the wave function. To retrieve the effect from the excited states, it was simulated by a van Vleck susceptibility χ_{VV} that yields a contribution to M_{Ln} linearly proportional to the applied magnetic field.

Finally, the angular averaging of magnetization was performed by calculating the magnetization for different fixed field directions $[M(\theta,\varphi)]$, uniformly distributed in the angular space since the molecules are randomly oriented with respect to the applied field. Then, the $M(\theta,\varphi)$ results were averaged. Each direction of the applied field is defined by the colatitude (θ) and azimuth (φ) angles. With the φ angle uniformly distributed in the $[0, 2\pi]$ interval and the colatitude θ in the $[-\pi, \pi]$. The interval value was chosen so that the average $M_{\text{th}}(H)$ reaches convergence within 0.1 μ_B.

V. EXPERIMENTAL RESULTS

A. XAS and XMCD at constant field

The XMCD spectra obtained at the L_2 and L_3 edges of Ln = Tb and Ho on the corresponding $\{Fe_3LnO_2\}$ complexes, measured at a temperature of 2.7 and 2.2 K, for the Tb and Ho compounds, respectively, under an applied magnetic field of 17 T, are displayed in Fig. 2. The XAS spectra have been normalized taking into account the statistical ratio of the L_3 to L_2 edge jump, i.e., $R = 2$ the ratio corresponding to the degeneracy of the corehole states and a total $L_{2,3}$ edges jump of 1.5.

The L_3-edge XMCD spectra of both Tb and Ho compounds consist of a negative dip followed by a main positive peak above the Fermi energy. Such negative dip is nearly imperceptible for the Tb case. This spectral feature has been associated to a quadrupolar transition (E2) that should be present at the L_3-edge spectra of heavy rare earths [29,30]. By comparison of the L_3-edge XMCD spectra of the Dy and Gd compounds

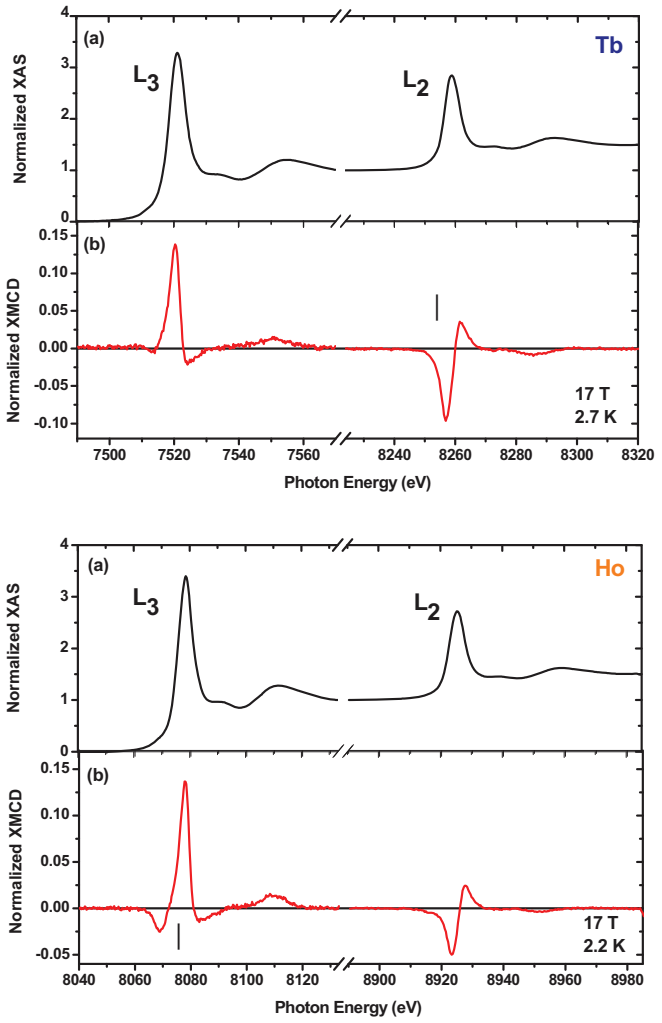

FIG. 2. (Color online) (a) XAS spectra and (b) XMCD signal at the Ln $L_{2,3}$ edges in $\{Fe_3LnO_2\}$ compounds for Ln = Tb (top) and Ho (bottom). Vertical lines indicate the chosen photon energy for the $I_{XMCD}(H)$ measurements.

(Fig. 4 of Ref. [10]) with the present ones it can be realized that the amplitude of such negative peak increases as the Ln atomic number increases. In fact, its magnitude is largest for the heaviest Ln, i.e., Ho, and the smallest corresponds to the Tb case, being that of the Dy an intermediate value. On the other hand, the main positive peak is of dipolar origin and its magnitude remains constant for the different Ln substitutions.

The L_2-edge XMCD spectra of the two $\{Fe_3LnO_2\}$ complexes consist of a main negative peak above the edge and a smaller positive peak at higher energy. An additional feature consisting of a negative shoulder at $E = 8915$ eV appears for Ln = Ho, but not for Tb. Comparing the L_2-edge XMCD spectra of the Dy and Gd compounds (Fig. 4 of Ref. [10]) with the present ones, we realize that the amplitude of the $\{Fe_3LnO_2\}$ spectra decreases as the lanthanide atomic number increases.

The shape and magnitude of the $L_{2,3}$ edges XMCD spectra of the $\{Fe_3TbO_2\}$ and $\{Fe_3HoO_2\}$ complexes (Fig. 2) are comparable with those in binary $TbAl_2$ and $HoAl_2$ compounds [31], and the Al-rich $Ln(Al_{1-x}Fe_x)$ compounds (with Ln = Tb and Ho) [32]. In heavy rare-earths ions, the positive L_3 and negative L_2 peaks indicate that the average rare-earth moment is polarized in the direction of the applied field. Then, in our case, we may assert that the Ln moment in both compounds $\{Fe_3TbO_2\}$ and $\{Fe_3HoO_2\}$ remains parallel to the applied field at the measured temperature ($T \approx 2.5$ K) and fields ($B \approx 17$ T).

The contribution of the quadrupolar ($2p \rightarrow 4f$) transitions [29,33–35] together with the spin dependence of the radial matrix elements of the dipolar ($2p \rightarrow 5d$) transitions [36,37] affect the XMCD signal at the Ln $L_{2,3}$ absorption edges. Consequently, the sum rules cannot be used to analyze the $L_{2,3}$ edges XMCD of lanthanide elements. Therefore the absolute spin and orbital moments of the Ln = Tb and Ho cannot be determined from the XMCD experiment.

B. XMCD as a function of the field

It is important to remark that since the intra-atomic $4f$-$5d$ exchange interaction is positive for the heavy rare earths [16], the evolution with the field of the XMCD signal at the $L_{2,3}$ edges can be considered directly proportional to the local magnetization from the $4f$ states.

In order to obtain a magnetization curve from the XMCD measurement, we need to record the XMCD signal as a function of the field, $I_{XMCD}(H)$, at a fixed energy. For the Tb case, where lower edge energies are involved, the L_2 edge of Tb ($E = 8257$ eV) was selected to avoid any interference from the EXAFS oscillations of Fe. However, in the Ho case, we selected the specific energy that corresponds to the maximum amplitude of the XMCD signal at the L_3 edge of Ho, $E = 8078$ eV.

The element-specific magnetization curves are depicted in Fig. 3. They reveal that the magnetization of the Tb(III) and Ho(III) ions is always oriented parallel to the applied magnetic field, as indicated by the sign of the $I_{XMCD}(H)$ signal for both the Tb and Ho compounds. We conclude that in the $\{Fe_3LnO_2\}$ compounds so far studied (Ln = Gd, Tb, Ho, and Dy), the Ln ion dominates the total magnetization of the cluster.

C. Magnetization versus field

The cluster magnetization curves $M_{tot}(H)$ of the $\{Fe_3TbO_2\}$ and $\{Fe_3HoO_2\}$ compounds, measured with a PPMS measurement platform with a vibrating sample magnetometer (VSM) option, at $T = 2.7$ and 2.2 K, respectively, and a magnetic field up to 14 T, are plotted in Figs. 4(a) and 4(b).

VI. DISCUSSION

A. Magnetic contributions of the lanthanide and Fe_3 subclusters

From the results of XMCD and $M(H)$, the contribution of the two subcluster components, Ln and Fe_3, which make up the total magnetization of the cluster $M_{tot}(H)$, were determined separately. On the one hand, the total magnetization of the cluster, $M_{tot} = M_{Ln} + M_{Fe_3}$ was obtained from the VSM measurements in absolute scale; i.e., in μ_B per formula unit (f.u.). On the other hand, the XMCD measured intensity, $I_{XMCD}(H)$, was obtained in arbitrary units. From these two sets of data, the magnetization contributed by the Ln ions,

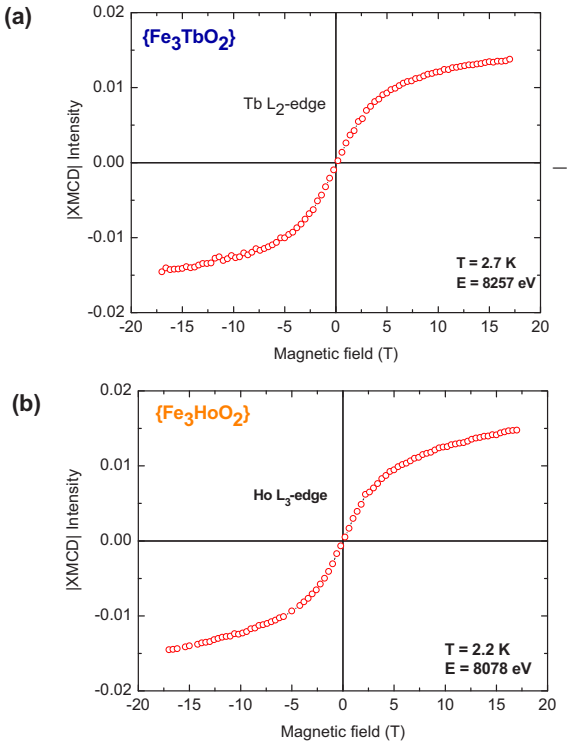

FIG. 3. (Color online) Collected magnetization curves as a function of applied field from XMCD experimental data at fixed energy in the $\{Fe_3LnO_2\}$ compounds: (a) for Ln = Tb, at $T = 2.7$ K, L_2 edge at $E = 8257$ eV; and (b) for Ln = Ho, at $T = 2.2$ K, L_3 edge at $E = 8078$ eV.

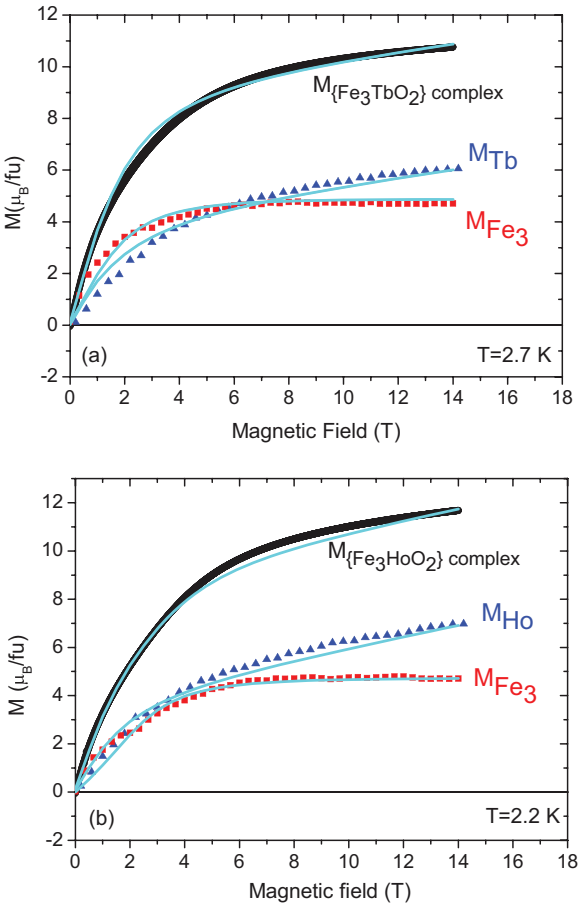

FIG. 4. (Color online) $M(H)$ curves of $\{Fe_3LnO_2\}$ compounds with Ln = Tb (a) and Ho (b). Macroscopic $M_{tot}(H)$ curve obtained from VSM measurements at $T = 2.7$ and 2.2 K, for Tb and Ho compounds, respectively (●). Microscopic magnetization curve obtained from XMCD at the L_2 and L_3 edges, respectively (▲). Magnetization of the total Fe present in the system obtained by subtraction of the two previous curves (■). $M^{th}(H)$ predictions for Tb (a) and Ho (b) (–), at $T = 2.7$ and 2.2 K, respectively.

M_{Ln}, can be determined in μ_B/f.u. by scaling $I_{XMCD}(H)$ of Fig. 3, as explained below.

At the highest magnetic field $B = 14$ T, where both VSM and XMCD magnetization data were available, the M_{Fe_3} subcluster is completely saturated $M^s_{Fe_3} = 4.70(5)$ μ_B/f.u., as found for the $\{Fe_3YO_2\}$ complex (Fig. 8) [10,19]. Since the contributions to the magnetization from the Fe_3 and Ln subsystems are additive at any field, the magnetization M_{Ln} at that high field (hf) can be calculated by subtracting $M^{hf}_{Ln} = M_{tot}(14T) - 4.70$ μ_B/f.u. Thus we obtained $M^{hf}_{Tb} = 5.8(2)$ μ_B/f.u. and $M^{hf}_{Ho} = 7.0(2)$ μ_B/f.u. Then, the scaling factor β could be calculated as $\beta = M^{hf}_{Ln}/I_{XMCD}(H_{hf})$. In this manner, the factors $\beta = 460$ and 500 μ_B/(Normalized XMCD units) were obtained for $\{Fe_3TbO_2\}$ and $\{Fe_3HoO_2\}$, respectively. With these values the local magnetization curve of each Ln, $M_{Ln}(H)$, was calculated for Tb and Ho, respectively [Figs. 4(a) and 4(b), filled triangles].

Finally, the magnetization curve of the Fe_3 subcluster as a function of the field, M_{Fe_3}, can be calculated as $M_{Fe_3}(H) = M_{tot}(H) - M_{Ln}(H)$. The $M_{Fe_3}(H)$ data obtained for the Ln = Tb and Ho compounds are collected in Figs. 4(a) and 4(b), respectively.

B. Ln-Fe_3 exchange interaction

1. $\{Fe_3TbO_2\}$ *cluster*

For the calculation of the $M(H)$ components, we chose as a quantization axis of the electronic wave functions the direction of the Tb EAM, the x axis. Working in the fictitious spin $S^*_{Tb} = 1/2$ formalism for the Tb ion implies that the exchange Hamiltonian can be considered Ising type, i.e., $\hat{H}_{Tb\text{-}Fe_3} = -2\mathcal{J}^*_{FeTb,x} S^*_{Tb,x} \cdot S_{Fe_3,x}$. A linear van Vleck contribution $M_{vv}(H) = \chi_{vv} H$ was added to account for the linear increase observed in the high field $M_{Tb}(H)$ data, which is caused by the mixing of the ground state with the excited states. We achieved a sound fit for the two experimental contributions, $M_{Fe_3}(H)$ and $M_{Tb}(H)$ simultaneously and, obviously for the total $M_{tot}(H)$ [Fig. 4(a)], using the theoretical model of Eq. (10). The fitted parameters, g^* components, $\mathcal{J}^*_{FeTb}$ components and Δ^{exp} are given in Table I. The exchange constant obtained from the fit is $\mathcal{J}^*_{FeTb,x}/k_B = -1.5(1)$ K and the doublet splitting is $\Delta^{exp}/k_B = 5.0(1)$ K, which is in reasonable agreement with that predicted by the *ab initio* calculations ($\Delta/k_B = 3.17$ K). The fit supports the condition of $g^*_\perp = 0$, as expected for a non-Kramers ion, i.e., Tb retains a strong uniaxial character when coupled to the Fe_3 subcluster. In spite of the overall general resemblance of the fitted curve to the data, some shortcomings are observed, such as an underestimation of the calculated $M_{Ln}(H)$ at high field ($B >$

TABLE I. Parameters used in the fit of all the $M(H)$ curves at low temperature ($T = 2.7$ and 2.2 K, for the Tb and Ho cases, respectively) with the theoretical model]Eq. (10)]. The van Vleck susceptibility parameter was $\chi_{vv} = 0.15(1)$ and $0.24(2)\ \mu_B T^{-1}/f.u.$ for $\{Fe_3TbO_2\}$ and $\{Fe_3HoO_2\}$ compounds, respectively.

Ln	S^*_{Ln}	g^*_x	g^*_y	g^*_z	$\mathcal{J}^*_{FeLn,x}/k_B$ (K)	$\mathcal{J}^*_{FeLn,y}/k_B$ (K)	$\mathcal{J}^*_{FeLn,z}/k_B$ (K)	Δ^{exp}/k_B (K)
Tb	1/2	17.5(1)	0	0	−1.5(1)			5.0(1)
Ho	1/2	0.5(1)	0.5(1)	15.6(1)	0.4(1)	0.4(1)	−2.8(1)	10.0(2)

6 T). It may be caused by simplicity of the linear van Vleck term that takes account of the mixing of the excited states.

The energy levels scheme of the ground state multiplet for a single Tb(III) ion affected only by ligand field interactions and calculated *ab initio*, is shown in Fig. 5(a), to be compared with the energy levels scheme of the $\{Fe_3TbO_2\}$ cluster, i.e., once that the Tb ion is antiferromagnetically coupled with the Fe_3 subcluster [Fig. 5(b)]. The exchange interaction between the Tb ion and the Fe_3 subcluster results in the following effects.

(i) The energy level scheme for the Tb-Fe_3 cluster is completely different from that provided by the crystal field for a single Tb ion (Ref. [26]). Indeed, the energy levels of the Tb-Fe_3 cluster [Fig. 5 (b)] are doubly Kramers degenerate, while those calculated by *ab initio* for the single ion are singlets.

(ii) At $H = 0$, the ground state of the entire cluster is a Kramers doublet $|\varepsilon_0\rangle$, $|\varepsilon_1\rangle$ dominated by the total cluster spin wave functions $|J^*, M^*_J\rangle = |2, \pm 2\rangle$ (see Sec. IV). At $H = 0$, the expectation values of all components of the S_{Fe_3} and S^*_{Tb} spins are zero.

For $\mu_0 H \neq 0$, the evolution of the energy levels scheme with the intensity of the applied field and the calculated total magnetization $M_{th}(H)$ parallel to the magnetic anisotropy axis of the molecular cluster are shown in Figs. 6(a) and 6(b), respectively.

At a field $\mu_0 H = 0.5$ T, aligned parallel to the EAM, the ground-state wave function, expressed as product wave functions, is dominated by $|S_{Fe_3}, m_{Fe_3}, S^*_{Tb}, m_{Tb}\rangle = |5/2, +5/2, 1/2, -1/2\rangle$, which indicates a probability of 97% of finding the spin configuration of antiparallel S_{Fe_3} and S^*_{Tb} orientation. Let us remember here that the expectation value $\langle S^*_{Tb,x}\rangle = -0.29$ in terms of the fictitious spin $S^* = 1/2$ implies an expectation value in real Tb spin $\langle J_{Tb,x}\rangle = -3.5$, and in terms of magnetization, $\langle M_{Tb,x}\rangle = 5.1\ \mu_B$ [Fig. 6(b)]. Therefore this ground state describes the quantum state where the average Tb magnetization is parallel to the applied field, and the Fe_3 magnetization is oriented opposite to the Tb one.

As the field increases, the wave function $|5/2, -5/2, 1/2, -1/2\rangle$, which originates from the excited multiplet

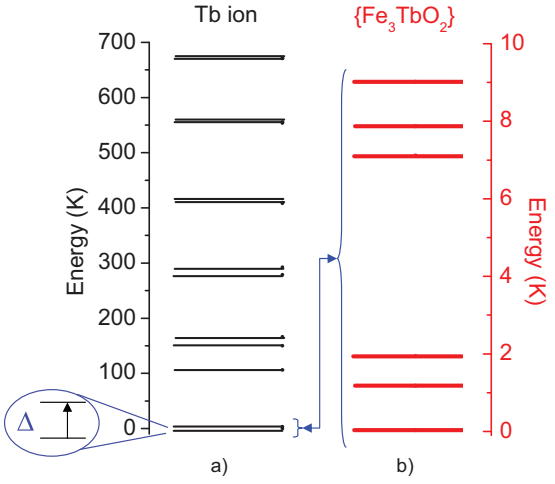

FIG. 5. (Color online) Energy levels of the ground multiplet of (a) a single Tb(III) ion, provided by the *ab initio* calculations (Ref. [26]) and (b) the $\{Fe_3TbO_2\}$ cluster, calculated with the parameters shown in Table I and $H = 0$.

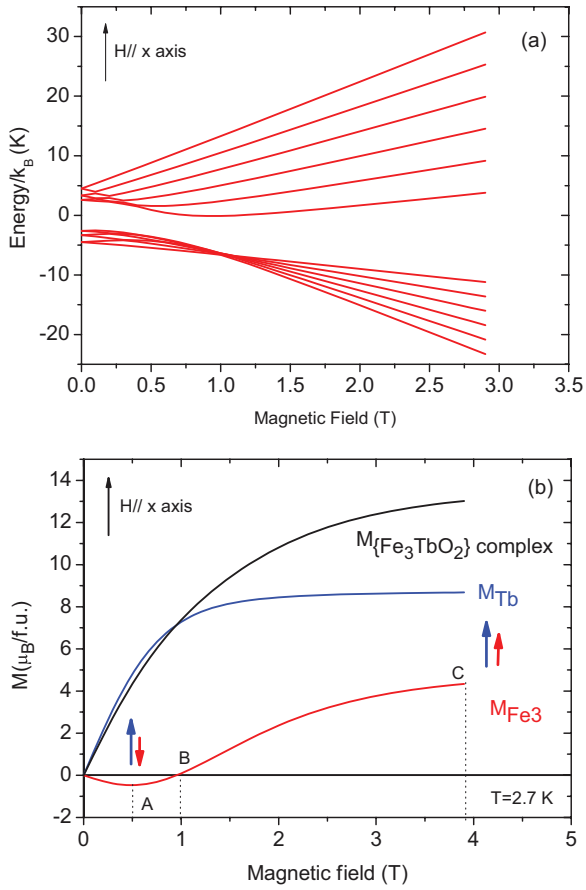

FIG. 6. (Color online) (a) The $\{Fe_3TbO_2\}$ energy level Zeeman splitting scheme for applied field parallel to the x direction. (b) The simulation of the $M_{th}(H)$ curves of the $\{Fe_3TbO_2\}$ compound with $g^*_x = 17.5$, $g^*_y = g^*_z = 0$, $\mathcal{J}^*_{FeTb,x}/k_B = -1.5$ K, and $\Delta^{exp}/k_B = 5.0$ K. Arrows indicate the average direction of the Tb (large ↑) and of Fe_3 subcluster (small ↑) moments at points A (antiparallel) and C (parallel), point B indicates the crossover field. Note that the magnetic moments (arrows) and the third component of the spin are opposite in sign.

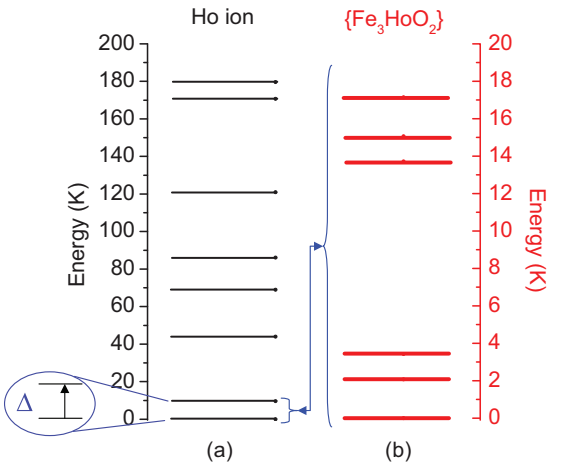

FIG. 7. (Color online) Energy levels of the ground multiplet of (a) a single Ho(III) ion, provided by the *ab initio* calculations (Ref. [26]) (only the eight lowest states are plotted) and (b) the $\{Fe_3HoO_2\}$ cluster, calculated with the parameters shown in Table I and $H = 0$.

at zero field, becomes dominant in the ground state. This means that the parallel spin configuration prevails and both Fe_3 and Tb spin expectation values are fully polarized on the direction of the field.

Figure 6(b) shows that the thermal averaged $M_{Fe_3}(H)$ curve dips to negative values for fields in the range $0 < \mu_0 H < 1.1$ T ($\mu_0 H = 0.5$ T, point A), which implies that the relative orientation of the thermally averaged magnetization expected values $\langle M_{Fe_3}\rangle$ and $\langle M_{Tb}\rangle$ are antiparallel in this field region. At $\mu_0 H = 1.1$ T (point B), there is a crossover to positive values, i.e., there is a reorientation of $\langle M_{Fe_3}\rangle$ from antiparallel to parallel with respect to $\langle M_{Tb}\rangle$.

It is concluded that the magnetization of the Tb dominates the total magnetization of the respective clusters. Indeed, because of the high anisotropy of Tb, the single ion anisotropy energy is dominant, therefore it establishes the quantization direction. The expectation value of the Ln moment at the ground state is maximum in the direction and sign of the applied field. That is, it is the applied field that determines the positive direction of the Ln magnetization direction. The Tb-Fe_3 antiferromagnetic exchange interaction generates an internal field on the Fe_3 subcluster antiparallel to the applied field, with a value $|\vec{B}_{\text{Ln-Fe}_3}| \approx 2\mathcal{J}_{\text{FeTb}}\mu_0 J_{\text{Tb}}/g_{\text{Fe}_3}\mu_B$. In terms of the real angular momenta $J_{\text{Tb}} = 6$, the internal fields $|\vec{B}_{\text{Tb}-\text{Fe}_3}| = 1.1$ T can be estimated for the Tb ion. Therefore the reorientation of the Fe_3 subcluster moment only succeeds when the external applied field is larger than the opposing exchange field $|\vec{B}_{\text{Tb-Fe}_3}|$. If the applied field is at an angle with respect to the anisotropy axis, only its projection onto the quantization direction opposes the internal field.

2. $\{Fe_3HoO_2\}$ *cluster*

Following the *ab initio* results for the Ho compound, the z axis (shown in Fig. 1) was chosen as quantization axis for the magnetization calculation of both sublattices, the Ho ion and Fe_3 subcluster. The experimental $M(H)$ curves of the Ho substitution were fitted using the Hamiltonian (10) with the fictitious spin $S^*_{\text{Ho}} = 1/2$ formalism. The two separated contributions $M_{\text{Ho}}(H)$ and $M_{Fe_3}(H)$, and the total $M_{\text{tot}}(H)$ were nicely fitted [Fig. 4 (b)] with the parameters given in Table I. A linear van Vleck contribution $M_{vv}(H) = \chi_{vv}H$ was also added to account for the linear increase observable in the high field $M_{\text{Ho}}(H)$ data. Contrary to the Tb substitution, which shows an Ising type interaction, in the $\{Fe_3HoO_2\}$ case, an anisotropic exchange interaction model ($\mathcal{J}_x = \mathcal{J}_y < \mathcal{J}_z$), albeit with dominant $\mathcal{J}_z$ interaction, was required to simulate the exchange interaction between the Ho ion and the Fe_3 subcluster.

The exchange interaction constants obtained from the fit are $\mathcal{J}^*_{\text{FeHo},z}/k_B = -2.8(1)$ K and $\mathcal{J}^*_{\text{FeHo},x}/k_B = \mathcal{J}^*_{\text{FeHo},y}/k_B = +0.4(1)$ K. Moreover, we did not obtain a perfect uniaxial anisotropy, since nonzero perpendicular components for the g^*_{Ho} tensor were required $g^*_{\text{Ho}} = (0.5, 0.5, 15.6)$ (Table I). Finally, the fitted splitting parameter $\Delta^{\text{exp}}/k_B = 10.0(2)$ K is in very good agreement with that predicted by *ab initio* calculations ($\Delta/k_B = 9.7$ K).

The component of the exchange interaction constant parallel to the common quantization z axis for the Ho and the Fe_3 subcluster $\mathcal{J}^*_{\text{FeHo},z}$ is antiferromagnetic and dominant, while the transverse components $\mathcal{J}^*_{\text{FeHo},x}$, $\mathcal{J}^*_{\text{FeHo},y}$ are weakly ferromagnetic.

The $\{Fe_3HoO_2\}$ case is similar to that of the $\{Fe_3DyO_2\}$ compound, since both lanthanides are uniaxial anisotropic and have their EAMs parallel to the quasisymmetry plane of the molecule. However, the $\{Fe_3HoO_2\}$ compound contains a non-Kramers ion Ho(III), while Dy(III) is a Kramers one. Because of the non-Kramers character of the single ion Ho ground state and first excited level, the parameter Δ is necessary to perform the fit, while it did not appear in the Dy case.

On the other hand, the Ho case is similar to Tb since both are non-Kramers ions with a ground-state uniaxial anisotropy. Therefore the quantum-mechanical description is that given in detail in Sec. IV. The differences are in the direction of the ground-state EAM, which is the z axis in the Ho case, and the real angular momentum of Ho, $J_{\text{Ho}} = 8$. (For Tb, the EAM is the x axis and $J_{\text{Tb}} = 6$.)

Figure 7 shows the energy levels scheme of the ground multiplet of a single Ho ion in comparison with that of the $\{Fe_3HoO_2\}$ cluster. The same behaviour as observed in the Tb case is reported.

In the Ho case, in order to determine the internal spin reorientation crossover fields, the simulation has been performed under the condition of the field applied in the z direction. At $T = 2.2$ K, the dependence on the applied field of the cluster eigenfunctions, eigenstates, $\langle M_{Ho,z}\rangle$, and $\langle M_{\text{Fe}_3,z}\rangle$ are analogous to the results for Tb depicted in Fig. 6, albeit for the EAM, which is z in the Ho case.

At fields $0 < \mu_0 H < 2.1$ T, the Fe_3 magnetic moment remains antiparallel to the field direction, as indicated by the negative values obtained for the averaged $M_{Fe_3}(H)$ curve of the Ho compound. At $\mu_0 H = 2.1$ T, the reorientation of the $\langle M_{Fe_3}\rangle$ moment in the field direction takes place, giving positive values in the corresponding $M_{Fe_3}(H)$ curve.

In the $\{Fe_3TbO_2\}$ molecule, the condition of $g^*_{\perp,Tb} = 0$, obtained from the Ln single ion *ab initio* calculations, is satisfied by the fit to the experimental data of the coupled Fe_3-Tb cluster. In fact, for non-Kramers ions, the ground-state anisotropy is expected to be strongly uniaxial, $g^*_{\perp,Ln} = 0$, due to time-reversal symmetry arguments, if $\Delta \ll E_2$ ($\Delta = 5$ K,

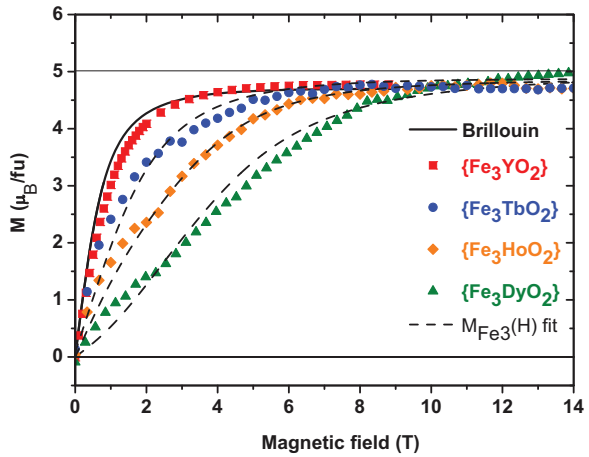

FIG. 8. (Color online) $M_{\rm tot}(H) \equiv M_{\rm Fe_3}(H)$ data of $\{Fe_3YO_2\}$ (□) and $M_{\rm Fe_3}(H)$ curves of the uniaxial anisotropic clusters $\{Fe_3DyO_2\}$ (△), $\{Fe_3TbO_2\}$ (○), and $\{Fe_3HoO_2\}$ (◇), and their correspondent simulated curves $M^{\rm th}_{\rm Fe_3}(H)$ (dashed lines).

$E_2 = 109$ K), i.e., the second excited states are very high in energy with respect to Δ (Ref. [27]). In contrast, in $\{Fe_3HoO_2\}$ the ratio $g^*_{\perp,Ho}/g^*_{Z,Ho} = 0.03$, is small but nonzero. Of course, this is not violating the previously mentioned condition for non-Kramers ions, but rather means that the higher excited levels are not so far in energy ($\Delta = 10$ K, $E_2 = 45$ K) and there is some mixing from the excited states in the Ho wave functions. The calculated $M_{\rm Ln}(H)$ at high fields is underestimated, just as in $\{Fe_3TbO_2\}$.

Although from the *ab initio* calculations, the data analysis and fit to the model, one concludes that the Ho case is representative for anisotropic exchange interaction rather than just Ising interaction, the perpendicular components of exchange are very small in comparison to the main component; therefore the $\{Fe_3HoO_2\}$ cluster can be considered to a good approximation as uniaxial anisotropic.

3. *Comparison between uniaxial* $\{Fe_3LnO_2\}$ *exchange interactions*

The $M_{\rm Fe_3}(H)$ data obtained for the Tb and Ho compounds are collected in Fig. 8 together with the data for the Dy compound. The $M(H)$ curve of the $\{Fe_3YO_2\}$ is included for comparison to a nonmagnetic Ln ion. It is qualitatively evidenced from Fig. 8 that the effect of substituting the nonmagnetic Y by a heavy rare earth as Tb, Ho, and Dy is to decrease the polarizability of the Fe_3 subcluster magnetic moment in the trend $\{Fe_3YO_2\}>\{Fe_3TbO_2\}>\{Fe_3HoO_2\}>\{Fe_3DyO_2\}$, because of the compensating effect of an intracluster Ln-Fe_3 antiferromagnetic coupling. Though the trend of the Fe_3 moment polarizability is well described by the model simulations for $M_{\rm Fe_3}(H)$, they are systematically lower than the experimental data at $B < 2$ T. The reason for the discrepancy lays probably in the incomplete fulfillment of angular random orientation of the crystallites in the powder sample.

Indeed, Table II allows us to compare the Ln-Fe_3 effective exchange constants obtained for the different compounds, when the fictitious spin $S^*_{\rm Ln} = 1/2$ (Ln = Tb, Ho, and Dy) formalism is used. We conclude that as the effective $\mathcal{J}^*_{\rm FeLn}$ constant increases, the magnetization of the Fe_3 sublattice needs a higher magnetic field to reach saturation. In fact, at $H = 0$, the intracluster exchange anisotropy can be calculated from the values of $J_{\rm FeLn}$ deduced from the present work and from Ref. [10] and expressed in terms of the real angular moment ($J_{\rm Ln}$) as

$$\Delta E_{\rm ex}/k_{\rm B} = 4\frac{\mathcal{J}_{\rm FeLn}}{k_{\rm B}}|S_{\rm Fe_3}||J_{\rm Ln}|, \qquad (12)$$

which amounts to $\Delta E_{\rm ex}/k_{\rm B} = 8.75$, 7.80, 14.4, and 30.0 K for Gd, Tb, Ho, and Dy, respectively.

The anisotropy introduced by the Ln ion to the cluster affects the mechanism of the intracluster interaction. Indeed, for the Ln = Tb substitution, an Ising-type interaction is considered, while in the Dy and Ho cases, an anisotropic type is required ($\mathcal{J}_x = \mathcal{J}_y < \mathcal{J}_z$). Specifically, we have obtained exchange interaction values $\mathcal{J}_{\rm FeTb}/k_{\rm B} = -0.13(1)$ K for the Ln = Tb substitution, $\mathcal{J}_{\rm FeHo}/k_{\rm B} = -0.18(1)$ K for Ln = Ho and $\mathcal{J}_{\rm FeDy}/k_{\rm B} = -0.40(1)$ K for Ln = Dy, expressed in terms of the real Ln spin, $J_{\rm Tb} = 6$, $J_{\rm Ho} = 8$, and $J_{\rm Dy} = 15/2$, respectively. The Ln anisotropy has an important effect on the relative orientation of the Ln and Fe_3 magnetizations.

C. Comparison to other *d-f* complexes

The exchange interaction results of the $\{Fe_3TbO_2\}$ and $\{Fe_3HoO_2\}$ compounds may be compared to other *d-f* complexes involving Tb(III) and Ho(III) reported in the literature with the help of Table II. We compare our results with other M = Fe(III) complexes, and below, for completeness sake, with Ln-transition metal M = Cu, Ni, and Co compounds.

Figuerola *et al.* [38] reported a study of the magnetic susceptibility of several complexes belonging to the families $[Ln(III)(DMF)_4(H_2O)_3(\mu\text{-}CN)Fe(III)(CN)_5]\cdot nH_2O$ with Ln = Gd(III), Dy(III), Tb(III) and Ho(III). They found that the Ln(III)-Fe(III) interaction was antiferromagnetic for Ln = Gd and Dy and ferromagnetic for Ln = Tb and Ho.

The family of tetranuclear heterometallic assemblies, $[Fe(III)_2Ln_2(H_2L)_4(\eta^2\text{-}NO_3)_2]2ClO_4 2CH_3OH 2H_2O$ with Ln = Gd(III), Dy(III), and Tb(III) was studied by Bag *et al.* [39]. Magnetic measurements revealed the presence of predominant ferromagnetic coupling for all the three compounds at low temperature.

It is interesting to note that the structural data of the studied $[Cu(II)LTb(III)(hfac)_2]_2$ compound [40] revealed that the local symmetry of the Tb ions in the Cu_2Tb_2 complex was very low, as occurs now for the Ln(III) ions in the present studied butterfly molecules. From the XMCD measurements performed on the Tb $M_{4,5}$ edges of the Cu_2Tb_2 compound at $T = 2$ K and $H = 70$ kOe, they obtained a total magnetic moment of 5.8(2) $\mu_{\rm B}/at.$ for the Tb(III) ions in the Cu_2Tb_2 molecule. This value coincides exactly with the magnetization value at high field (14 T) found for the Tb ion in the present $\{Fe_3TbO_2\}$ compound, $M^{\rm hf}_{\rm Tb} = 5.8(2)$ $\mu_{\rm B}$/f.u. [Fig. 4(a) (▲)]. As we have shown in Sec. VI B, this value is explained as the saturation magnetization of a collection of uniaxial highly anisotropic molecules ($M_s = \frac{1}{2}\mu = 4.3$ $\mu_{\rm B}$) and a Van Vleck contribution due to mixing of excited levels. This interpretation contradicts the argument given in Ref. [40] that the moment reduction is due to crystal field effects. Those authors do not consider the random orientation of the crystallites.

TABLE II. Comparison of exchange interaction constants in d-f complexes. Recall that $\mathcal{J}^*$ is the exchange interaction in the fictitious $S^* = 1/2$ formalism.

Compound	Exchange interaction	Ref.
$\{Fe_3TbO_2\}$	$\mathcal{J}^*_{FeTb,x}/k_B = -1.5(1)$ K (VSM and XMCD)	This work
$\{Fe_3HoO_2\}$	$\mathcal{J}^*_{FeHo,z}/k_B = -2.8(1)$ K (VSM and XMCD) $\mathcal{J}^*_{FeHo,x}/k_B = \mathcal{J}^*_{FeHo,y}/k_B = 0.4(1)$ K	
$\{Fe_3YO_2\}$	0	
$\{Fe_3DyO_2\}$	$\mathcal{J}^*_{FeDy,z}/k_B = -5.5(1)$ K (VSM and XMCD) $J^*_{FeDy,x}/k_B = \mathcal{J}^*_{FeDy,y}/k_B = 2.3(1)$ K	Badía-Romano *et al.* [10]
$\{Ln(III)(DMF)_4(H_2O)_3(\mu\text{-}CN)Fe(III)(CN)_5\}$	AF for Ln = Gd,Dy and FM for Ln = Tb, Ho (MSUS)	Figuerola *et al.* [38]
$\{Fe(III)_2Tb_2(H_2L)_4(\eta^2\text{-}NO_3)_2\}\cdot 2ClO_4 2CH_3OH 2H_2O$	FM	Bag *et al.* [39]
$\{Cu(II)LTb(III)(hfac)_2\}_2$	FM (MSUS)	Osa *et al.* [11]
$\{Cu(II)LTb(III)(hfac)_2\}_2$	FM (SQUID and XMCD)	Hamamatsu *et al.* [40]
$\{Cu_2Tb_2\}$	$\mathcal{J}^*_{ex,1}/k_B = 4.1$ K (INS) $\mathcal{J}^*_{ex,2}/k_B = 0.92$ K	Klokishner *et al.* [41]
$\{TbCuC_{19}D_{20}N_3O_{16}\}$	$\mathcal{J}^*_{ex,xy}/k_B = -6.38$ K (TOFNS) $\mathcal{J}^*_{ex,z}/k_B = -3.46$ K	Kofu *et al.* [42]
$\{TbCu_3\}$	$\mathcal{J}^*_{Tb-Cu}/k_B = 2.2(7)$ K (INS)	Kettles *et al.* [43]
$\{CuLn\}$ (Ln = Gd, Tb, Dy, Ho and Er)	FM	Costes *et al.* [44]
$\{Ln_2[Cu(opba)]_3\}$ (Ln = Tb, Ho)	AF	Kahn *et al.* [45]
$\{Ln_2M_3\}$ (Ln = Tb, Ho and M = Cu, Zn)	$J^*_{Tb-Cu}/k_B = 5.6$ K (LT-MSUS and HC) $\mathcal{J}^*_{Ho-Cu}$ very weak	Evangelisti *et al.* [46]
$\{Ln_2[Ni(opba)\}_3]\}$	FM for Ln=Tb(III) and perhaps Ho(III)	Khan *et al.* [47]
$\{L_2Co_2Tb(III)\}(NO_3)$	FM	Chandrasekar *et al.* [12]
$\{L_2Co_2Tb\}(NO_3)$	$\mathcal{J}^*_{Tb-Co}/k_B \approx 0.99$ K (MSUS)	Reu *et al.* [48]

FM: ferromagnetic; AF: antiferromagnetic.
VSM: VSM magnetometry; XMCD: x-ray magnetic circular dichroism; TOFNS: time-of-flight neutron spectroscopy; MSUS: magnetic susceptibility; SQUID: SQUID magnetometry; INS: Inelastic neutron scattering spectroscopy; LT-MSUS and HC: low temperature magnetic susceptibility and heat capacity.

From this revision, one concludes that both the Tb-transition metal and Ho-transition metal interactions may be ferro- or antiferromagnetic, depending on the actual cluster structure and bonds involved. At any rate, the Ln-metal interaction is very weak in the case of Ln = Tb and Ho.

VII. CONCLUSIONS

The combination of bulk magnetic techniques (VSM magnetometries) with spectroscopic techniques (XMCD) has allowed to analyze the intramolecular interaction at a macroscopic and microscopic level. This has enabled to evaluate the effect of the Ln ion and the Fe_3 subcluster contributions separately. Moreover, the comparison of the different Ln substitutions on the "butterfly" molecules series has allowed to evaluate the effect that the Ln anisotropy has on the magnetic interactions within the molecule.

It has been demonstrated that for the "butterfly" molecules containing a non-Kramers Ln ion, the fictitious $S^* = 1/2$ formalism can be applied to define an *ad hoc* effective spin Hamiltonian of the cluster. Therefore, in the framework of an effective exchange interaction model, between the trinuclear Fe_3 subcluster and the non-Kramers Ln ions, low-temperature magnetization as a function of field has been fitted in terms of a Ln-Fe_3 exchange constant. The fits show that the interaction between the Ln ion and Fe_3 subcluster is weakly antiferromagnetic for all the compounds in the series. Specifically, we have obtained $\mathcal{J}_{FeTb}(J_{Tb} = 6)/k_B = -0.13(1)$ K for the Ln = Tb substitution and $\mathcal{J}_{FeHo}(J_{Ho} = 8)/k_B = -0.18(1)$ K for Ln = Ho.

The Fe_3 magnetic moment undergoes a spin reorientation within the molecule from antiparallel to parallel orientation with respect to the Ln moment as the magnetic field increases. This reorientation is complete for an applied field larger than a threshold value directly related to the increasing antiferromagnetic interaction J_{FeTb} in the trend Tb, Ho, and Dy. The model proposed has some shortcomings, namely, the strong simplification implied in assuming that the contribution to $M_{Ln}(H)$ due to mixing of the excited states is represented by an *ad hoc* linear term with the applied field, and that there may be a small departure from complete angular randomness in the powder crystallites. However, the Fe_3 and Ln magnetic moment polarization, opposed by the antiferromagnetic coupling, is correctly captured by the simple model used. We also conclude from this work that the possible SMM character of these molecules cannot show up unless a temperature region below 1 K is explored. The combination of the element selective XMCD and VSM have allowed us to determine the intracluster interactions and reorientation of the subcluster Fe_3 and Ln (non-Kramers ions) magnetic moments.

ACKNOWLEDGMENTS

Fruitful discussions with P. J. Alonso are acknowledged. The projects MINECO (MAT2011/23791, MAT2011/27233-C02-02, and MAT2014/53921-R), DGA IMANA E34, and

Alexander Von Humboldt Foundation (D.P.) are acknowledged for financial support. The XMCD data were taken during the training period of L.B. carried out in ID12 at the ESRF. The authors would like to acknowledge the use of Servicio General de Apoyo a la Investigación (SAI), Universidad de Zaragoza. We also thank resources from the supercomputer "Caesaraugusta," technical expertise and assistance provided by BIFI-Universidad de Zaragoza.

[1] J. R. Friedman, M. P. Sarachik, J. Tejada, and R. Ziolo, Phys. Rev. Lett. **76**, 3830 (1996).
[2] J. M. Hernández, X. X. Zhang, F. Luis, J. Bartolomé, J. Tejada, and R. Ziolo, Europhys. Lett. **35**, 301 (1996).
[3] L. Thomas, F. Lionti, R. Ballou, D. Gatteschi, R. Sessoli, and B. Barbara, Nature (London) **383**, 145 (1996).
[4] R. Sessoli, D. Gatteschi, A. Caneschi, and M. A. Novak, Nature (London) **365**, 141 (1993).
[5] M. N. Leuenberger and D. Loss, Nature (London) **410**, 789 (2001).
[6] R. Sessoli and A. K. Powell, Coord. Chem. Rev. **253**, 2328 (2009).
[7] N. Ishikawa, M. Sugita, T. Ishikawa, S. Koshihara, and Y. Kaizu, J. Am. Chem. Soc. **125**, 8694 (2003).
[8] X. L. Wang, L. C. Li, and D. Z. Liao, Inorg. Chem. **49**, 4735 (2010).
[9] S. D. Jiang, B. W. Wang, G. Su, Z. M. Wang, and S. Gao, Angew. Chem. Int. Ed. **49**, 7448 (2010).
[10] L. Badía-Romano, F. Bartolomé, J. Bartolomé, J. Luzón, D. Prodius, C. Turta, V. Mereacre, F. Wilhelm, and A. Rogalev, Phys. Rev. B **87**, 184403 (2013).
[11] S. Osa, T. Kido, N. Matsumoto, N. Re, A. Pochaba, and J. Mrozinski, J. Am. Chem. Soc. **126**, 420 (2004).
[12] V. Chandrasekhar, B. M. Pandian, J. J. Vittal, and R. Clérac, Inorg. Chem. **48**, 1148 (2009).
[13] M. Murugesu, A. Mishra, W. Wernsdorfer, K. A. Abboud, and G. Christou, Polyhedron **25**, 613 (2006).
[14] C. Garino, E. Borfecchia, R. Gobetto, J. A. van Bokhoven, and C. Lamberti, Coord. Chem. Rev. **277-278**, 130 (2014).
[15] G. van der Laan and A. I. Figueroa, Coord. Chem. Rev. **277-278**, 95 (2014).
[16] C. Giorgetti, E. Dartyge, F. Baudelet, and R.-M. Galéra, Phys. Rev. B **70**, 035105 (2004).
[17] C. Turta, D. Prodius, V. Mereacre, S. Shova, M. Gdaniec, Y. A. Simonov, V. Kuncser, G. Filoti, A. Caneschi, and L. Sorace, Inorg. Chem. Comm. **7**, 576 (2004).
[18] V. Mereacre, D. Prodius, C. Turta, S. Shova, G. Filoti, J. Bartolomé, R. Clérac, C. E. Anson, and A. K. Powell, Polyhedron **28**, 3017 (2009).
[19] J. Bartolomé, G. Filoti, V. Kuncser, G. Schinteie, V. Mereacre, C. E. Anson, A. K. Powell, D. Prodius, and C. Turta, Phys. Rev. B **80**, 014430 (2009).
[20] A. Rogalev, J. Goulon, C. Goulon-Ginet, and C. Malgrange, in *Magnetism and Synchrotron Radiation*, edited by E. Beaurepaire, F. Scheurer, G. Krill, and J. P. Kappler, Lecture Notes in Physics Vol. 565 (Springer, Berlin, 2001), p. 60.
[21] B. O. Roos and P. A. Malmqvist, Phys. Chem. Chem. Phys. **6**, 2919 (2004).
[22] F. Aquilante, L. D. Vico, N. Ferre, G. Giovanni, P. Malmqvist, P. Neogrady, T. B. Pedersen, M. Pitonak, M. Reiher, B. O. Roos, L. Serrano-Andres, M. Urban, V. Veryazov, and R. Lindh, J. Comp. Chem. **31**, 224 (2010).
[23] K. Bernot, J. Luzón, L. Bogani, M. Etienne, C. Sangregorio, M. Shanmugam, A. Caneschi, R. Sessoli, and D. Gatteschi, J. Am. Chem. Soc. **131**, 5573 (2009).
[24] G. Cucinotta, M. Perfetti, J. Luzon, M. Etienne, P. E. Car, A. Caneschi, G. Calvez, K. Bernot, and R. Sessoli, Angew. Chemie. Int. Ed. **51**, 1606 (2012).
[25] J. Luzon and R. Sessoli, Dalton Trans. **41**, 13556 (2012).
[26] See Supplemental Material at http://link.aps.org/supplemental/10.1103/PhysRevB.92.064411 for description of the *ab initio* calculations results and the ground state wavefunctions of the $\{Fe_3LnO_2\}$ (Ln = Tb and Ho) cluster at $H = 0$.
[27] J. S. Griffith, Phys. Rev. **132**, 316 (1963).
[28] C. Rudowicz and M. Karbowiak, Coord. Chem. Rev. **287**, 28 (2015).
[29] F. Bartolomé, J. M. Tonnerre, L. Sève, D. Raoux, J. Chaboy, L. M. García, M. Krisch, and C. C. Kao, Phys. Rev. Lett. **79**, 3775 (1997).
[30] F. Bartolomé, M. H. Krisch, D. Raoux, and J.-M. Tonnerre, Phys. Rev. B **60**, 13497 (1999).
[31] M. A. Laguna-Marco, J. Chaboy, and C. Piquer, Phys. Rev. B **77**, 125132 (2008).
[32] M. A. Laguna-Marco, J. Chaboy, C. Piquer, H. Maruyama, N. Ishimatsu, N. Kawamura, M. Takagaki, and M. Suzuki, Phys. Rev. B **72**, 052412 (2005).
[33] J. C. Lang, S. W. Kycia, X. D. Wang, B. N. Harmon, A. I. Goldman, D. J. Branagan, R. W. McCallum, and K. D. Finkelstein, Phys. Rev. B **46**, 5298 (1992).
[34] J. C. Lang, G. Srajer, C. Detlefs, A. I. Goldman, H. König, X. Wang, B. N. Harmon, and R. W. McCallum, Phys. Rev. Lett. **74**, 4935 (1995).
[35] J. Chaboy, F. Bartolomé, L. M. García, and G. Cibin, Phys. Rev. B **57**, R5598 (1998).
[36] X. Wang, T. C. Leung, B. N. Harmon, and P. Carra, Phys. Rev. B **47**, 9087 (1993).
[37] B. N. Harmon and A. J. Freeman, Phys. Rev. B **10**, 1979 (1974).
[38] A. Figuerola, C. Diaz, J. Ribas, V. Tangoulis, J. Granell, F. Lloret, J. Mahía, and M. Maestro, Inorg. Chem. **42**, 641 (2003).
[39] P. Bag, J. Goura, V. Mereacre, G. Novitchi, A. K. Powell, and V. Chandrasekhar, Dalton Trans. **43**, 16366 (2014).
[40] T. Hamamatsu, K. Yabe, M. Towatari, S. Osa, N. Matsumoto, N. Re, A. Pochaba, J. Mrozinski, J.-L. Gallani, A. Barla, P. Imperia, C. Paulsen, and J.-P. Kappler, Inorg. Chem. **46**, 4458 (2007).
[41] S. I. Klokishner, S. M. Ostrovsky, O. S. Reu, A. V. Palii, P. L. W. Tregenna-Piggott, T. Brock-Nannestad, J. Bendix, and H. Mutka, J. Phys. Chem. C **113**, 8573 (2009).
[42] M. Kofu, O. Yamamuro, T. Kajiwara, Y. Yoshimura, M. Nakano, K. Nakajima, S. Ohira-Kawamura, T. Kikuchi, and Y. Inamura, Phys. Rev. B **88**, 064405 (2013).
[43] F. J. Kettles, V. A. Milway, F. Tuna, R. Valiente, L. H. Thomas, W. Wernsdorfer, S. T. Ochsenbein, and M. Murrie, Inorg. Chem. **53**, 8970 (2014).
[44] J.-P. Costes, F. Dahan, A. Dupuis, and J.-P. Laurent, Chem. A Eur. J. **4**, 1616 (1998).

[45] M. L. Kahn, C. Mathoniére, and O. Kahn, Inorg. Chem. **38**, 3692 (1999).

[46] M. Evangelisti, M. L. Kahn, J. Bartolomé, L. J. de Jongh, C. Meyers, J. Leandri, Y. Leroyer, and C. Mathonière, Phys. Rev. B **68**, 184405 (2003).

[47] M. L. Kahn, P. Lecante, M. Verelst, C. Mathonire, and O. Kahn, Chem. Mater. **12**, 3073 (2000).

[48] O. Reu, A. Palii, S. Ostrovsky, W. Wallace, O. Zaharko, V. Chandrasekhar, R. Clerac, and S. Klokishner, J. Phys. Chem. C **117**, 6880 (2013).